Study of Polymorphism of 4-Hexyl-4′-isothiocyanatobiphenyl by Complementary Methods

ARTICLE *in* THE JOURNAL OF PHYSICAL CHEMISTRY B · AUGUST 2011

Impact Factor: 3.3 · DOI: 10.1021/jp201936x

5 AUTHORS, INCLUDING:

Małgorzata Jasiurkowska-Delaporte
Institute of Nuclear Physics
17 PUBLICATIONS **128** CITATIONS
SEE PROFILE

Piotr M Zielinski
Polish Academy of Sciences
35 PUBLICATIONS **71** CITATIONS
SEE PROFILE

THE JOURNAL OF PHYSICAL CHEMISTRY B

ARTICLE

pubs.acs.org/JPCB

Study of Polymorphism of 4-Hexyl-4′-isothiocyanatobiphenyl by Complementary Methods

Małgorzata Jasiurkowska,*,† Piotr M. Zieliński,† Maria Massalska-Arodź,† Yasuhisa Yamamura,‡ and Kazuya Saito‡

†The Henryk Niewodniczanski Institute of Nuclear Physics, Polish Academy of Sciences, Radzikowskiego 152, Kraków 31-342, Poland

‡Department of Chemistry, Graduate School of Pure and Applied Sciences, University of Tsukuba, Tsukuba, Ibaraki 305-8571, Japan

ABSTRACT: The results of adiabatic calorimetry, mid-infrared spectroscopy, X-ray diffraction, and polarized microscopy of 4-hexyl-4′-isothiocyanatobiphenyl are presented. Apart from the well-known isotropic liquid and smectic phases, calorimetric measurements indicate the existence of two stable crystalline phases. Quantitative analysis of infrared bands enabled the determination of phase transitions, observation of crystallization kinetics, and elucidation of the glass transition of the crystal-like smectic E phase. The structural information about the glass of the smectic E obtained from the diffraction studies is complemented by textures recorded by polarized microscopy.

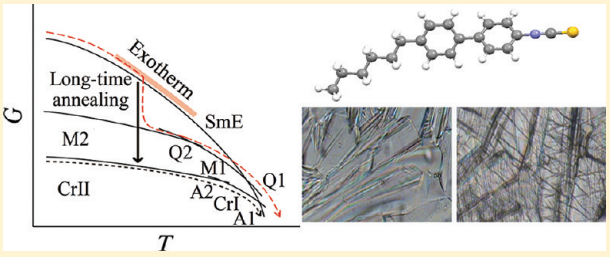

1. INTRODUCTION

The investigated substance belongs to the well-known 4-*n*-alkyl-4′-isothiocyanatobiphenyl homologous series (abbreviated as *n*TCB), which has been studied extensively by several measurement techniques.[1−18] The *n*TCB (n = 2−10) shows only one liquid crystalline phase: the crystal-like smectic E phase (SmE, labeled also as CrE), which is characterized by the orthorhombic arrangement of molecules orthogonal to the smectic layers. It has been found that in the SmE phase, there is long-range positional ordering of the molecular centers in the layer and between layers.[19−21] However, thermodynamic analysis for *n*TCB homologous series has pointed out an increase in the partial orientational disorder of the molecules and disorder of isothiocyanato and alkyl groups at the phase transition from the crystalline phase to the SmE phase.[22] Dielectric and NMR studies revealed that the molecules perform rotational motion around their principal axes. It was found that the end chains affect the molecular packing in the SmE phase and what follows the cooperative behavior of molecules in this mesophese.[2,3] Heat capacity measurements for the nTCBs with $n \leq 5$ revealed a strong influence of the alkyl chain length on the solid-state polymorphism. The 4TCB and 5TCB compounds show one and two crystalline stable phases, respectively, in addition to the SmE and isotropic phase. On the other hand, for 3TCB, a rich polymorphism in the solid state was found: five stable crystalline phases and the glass of the SmE phase.

In a previous paper, we reported the glass transition of the SmE phase of 3TCB for the first time.[18] We hypothesized that in the glass of SmE phase, the smectic layer system is sustained, but the orthorhombic order of the molecules in the layers is slightly disturbed. The vitreous state of the SmE phase is presumably formed by freezing the molecular reorientations and fluctuations of structural disorder. To elucidate the nature of the glassy state of highly ordered smectic phases, the systematic study for other substances is required.

The present paper reports a study of the polymorphism of 6TCB by means of several experimental techniques, that is, adiabatic calorimetry, mid-infrared spectroscopy, X-ray diffraction and polarizing microscopy, and DFT calculations at the B3LYP/6-31 level. The goal was to complete the phase pattern of the nTCBs and to compare the features of vitreous state of the SmE phase of 6TCB with those observed for 3TCB.

2. EXPERIMENTAL AND COMPUTATIONAL DETAILS

The 6TCB substance was synthesized according to ref 1 at the Institute of Chemistry, the Military University of Technology, Warsaw, Poland. The sample was crystalline at room temperature. Heat capacity measurements for 6TCB were performed using a laboratory-made adiabatic calorimeter, the details of which are described elsewhere.[23] The measurement was carried out by the so-called intermittent-heating adiabatic method in a heating direction from 6 K. The sample was loaded into a gold-plated calorimeter vessel. The vessel was sealed after introducing a small amount of helium gas (10^5 Pa at room temperature), which serves as the heat conduction gas inside the vessel. The thermal equilibrium inside the vessel was attained within the normal time (1−30 min, depending on temperature). The mass of the sample was 1.239 37 g (4.194 97 mmol) after the buoyancy correction. The sample contributed to the total heat capacity by 15% at 100 K, 12% at 200 K, and 15% at 300 K. The working thermometer was a platinum resistance thermometer (MINCO, Minneapolis, MN, S1059), the temperature scale of which is based upon the ITS-90.

Received: February 28, 2011
Revised: September 1, 2011
Published: September 08, 2011

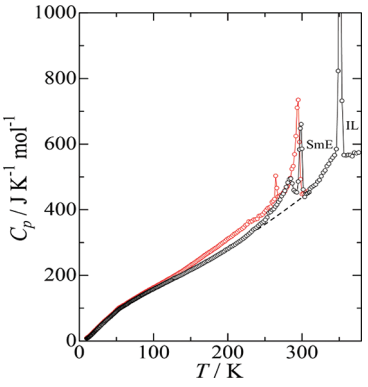

Figure 1. Heat capacities of the as-cooled (red) and the long-annealed (black) 6TCB.

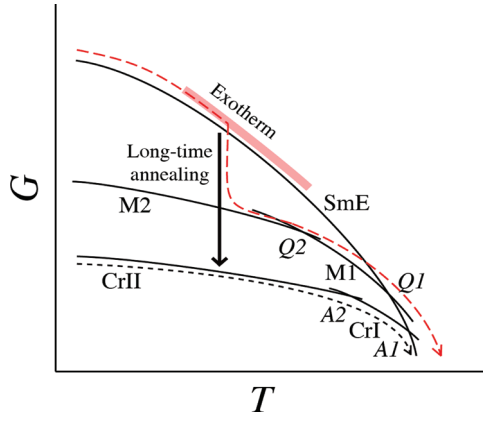

Figure 2. Gibbs energy vs temperature diagram deduced from the adiabatic calorimetry 6TCB. Red and black dashed lines indicate thermal trajectory of quenched and annealed 6TCB upon heating.

The IR spectra were obtained using an Excalibur FTS 3000 Fourier transform IR spectrometer in the wavenumber range of 4000−500 cm^{-1}. The sample was prepared by melting a substance between two KRS-5 plates separated by a Teflon ring with a thickness of 25 μm. Several experimental runs were performed on cooling and heating the substance in the temperature range 30−320 K.

Optical observations were performed by polarizing microscope Biopolar PI (PZO, Warsaw, PL) with Linkam (UK) THM 600 heating stage and TMS 90 controller on heating and cooling the substance in the temperature range 100−370 K.

X-ray studies were carried out on an X'Pert PRO (PANalytical, The Netherlands) diffractometer using the Cu Kα radiation (λ = 1.505 89 Å) and the graphite monochromator. The sample temperature was stabilized with an accuracy of ±0.1 K using a continuous flow cryostat supplied by Anton Paar Co. Details of sample preparation are given elsewhere.[3] Observations were performed each 10 K on heating the substance from 85 K.

2.1. Theoretical Calculations. Initial molecular geometry was optimized using the semiempirical AM1[24] method, as implemented by the MOPAC program. In the next step, further geometry optimization and calculations of frequencies and intensities of the vibration modes of the isolated molecule were performed with the Gaussian 09[25] program using density functional theory (DFT) at the B3LYP/6-31 level.[25] To obtain a better agreement

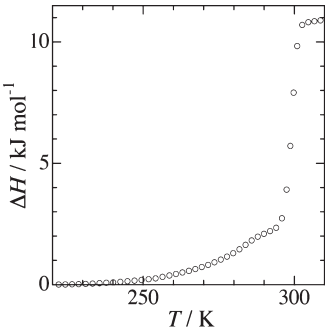

Figure 3. Excess enthalpy of two anomalies (A1 and A2) of 6TCB.

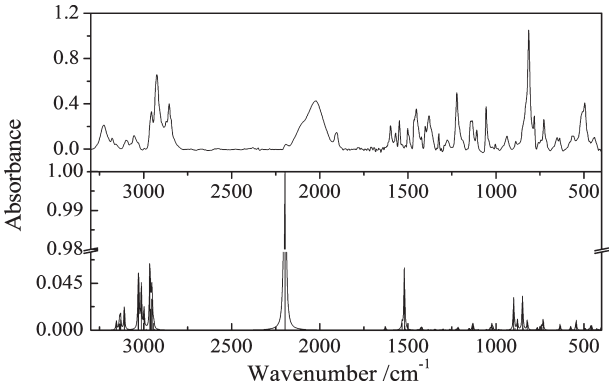

Figure 4. Experimental IR spectrum in the SmE phase of 6TCB at 318 K (top panel) and scaled IR spectrum predicted by DFT/B3LYP/6-31 (bottom panel).

between the DFT calculated vibrational frequencies and the experimental ones, the predicted values of frequencies were rescaled by a factor 0.985, estimated according to ref 18 and 26.

3. RESULTS AND DISCUSSION

3.1. Adiabatic Calorimetry. The heat capacities (C_p) of 6TCB are measured between 6 and 380 K in several runs for various thermal treatments of the sample. The resultant C_p's of the first and second runs are shown in Figure 1. In the first run, no special thermal treatment is applied before the measurement after cooling the sample to 82 K. A complicated thermal behavior is observed with increasing temperature. A strong heat evolution is encountered in the temperature region from 220 to 290 K. Such heat evolution has also been observed in the as-cooled samples of 3TCB[17] and 5TCB.[22] There is a slight anomaly with a latent heat at 264 K (Q2), in the middle of the exothermic region. The Q2 is probably due to a solid-to-solid phase transition (between M2 and M1 phases). After the exothermic region, another heat anomaly is found at 294 K (Q1) due to the phase transition from M1 phase to the SmE phase. Because of the heat evolution encountered, the sample was successively annealed at 250 K for four days and at 270 K for half a day until the heat evolution ceased completely. After the long annealing, the sample was cooled to 6 K, and the heat capacity was measured to 380 K (second run), as shown in Figure 1 by open circles. No heat evolution was detected in this run. The heat capacities of the annealed sample are smaller than those of the as-cooled one in the first run. Therefore, the annealed sample is probably in the

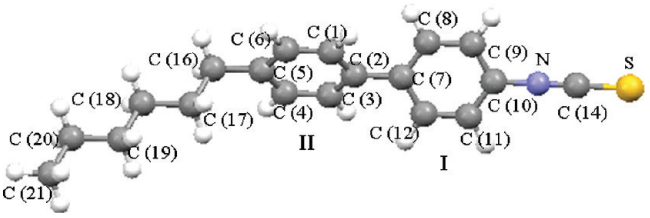

Figure 5. Geometry of the lowest energy conformation of the 6TCB molecule optimized by the DFT/B3LYP/6-31 method.

most stable crystalline phase. The annealed sample has only two heat anomalies at 284 K (A2) and 298 K (A1) up to the SmE phase. The A1 anomaly is accompanied by a latent heat and resulted from a phase transition from a crystalline phase (CrI) to the SmE phase. On the other hand, the A2 is a broad anomaly without a notable latent heat. The A2 anomaly presumably corresponds to a phase transition between two crystalline phases (CrII and CrI). Upon repeated rapid cooling of the sample from the SmE, the sample underwent phase transitions between the Q2 and the Q1 on ultimately reverting to the SmE phase. The temperatures of the A1 and A2 anomalies in the second run and of the Q1 and Q2 anomalies in the first run are clearly different.

Since those four anomalies are due to phase transitions, 6TCB has at least four polymorphs up to the SmE phase. The relation among the polymorphs is illustrated in the so-called Gibbs energy vs temperature diagram (Figure 2). Here, the A2 is treated as a first order phase transition for clarity of the diagram. Since the heat anomalies of the A1 and the A2 overlap each other, it is difficult to separate these anomalies. Assuming an interpolating curve between CrII and SmE as a baseline (Figure 1), we estimate the sum of excess enthalpy of the A1 and the A2 from the energy input to be ~11 kJ mol^{-1}, as shown in Figure 3. The heat anomaly at 350 K corresponds to the phase transition (clearing) from the SmE to isotropic liquid (IL) phase because the temperature is in quantitative agreement with the reported phase diagram.[2] The temperature, enthalpy, and entropy of this transition are (350.6 ± 0.1) K, (14.7 ± 0.1) kJ mol^{-1}, and (41.9 ± 0.1) J K^{-1} mol^{-1}, respectively. These thermodynamic quantities are consistent with the DSC results.[1]

3.2. Infrared Spectroscopic Studies. Figure 4 shows the IR spectra of SmE phase of 6TCB observed at 318 K in comparison with the simulated IR spectrum. The predicted (DFT) frequencies and intensities of the IR bands of 6TCB and the assignment of particular modes observed for the SmE phase, the glass of the SmE phase, and a crystalline phase CII are presented in Table 1 (see the Appendix). The computed structure of the lowest energy conformation of the 6TCB molecule is shown in Figure 5. The main structure parameters are reported in Table 2 (see the Appendix).

The range of the wavenumbers, ~3230−3007 cm^{-1}, corresponds mainly to the CH and CH_2 stretching vibrations. The broad band in the wavenumbers range from ~2200 to 1880 cm^{-1} is assigned to the ν_{as} (NCS) stretching modes (see Figure 4). The contribution from the vibration of the phenyl rings are dominant in at 1600−700 cm^{-1}. The lower wavenumbers region of 550−430 cm^{-1} corresponds to the NCS in-plane deformations and stretches. According to the DFT calculations, one can expect a single intensive band of ν_{as} (NCS) at 2251 cm^{-1}. The large width of ν_{as} (NCS) mode with additional peaks at ~2200−1880 cm^{-1} is commonly interpreted as an effect of the Fermi resonance between intramolecular stretching vibrations and combination

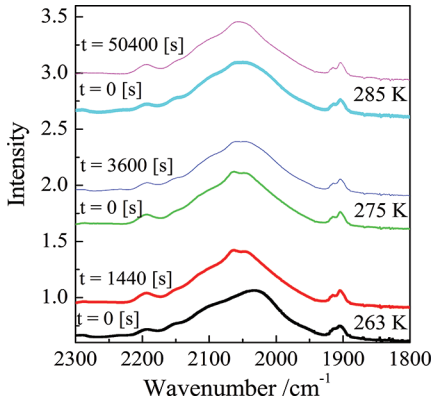

Figure 6. Profiles of the IR bands in the region of the NCS stretching vibration at 263, 275, 285 K. The spectra were recorded at the beginning (t = 0 s) and at the end of the annealing processes.

tones[27−30] and a resonance of the "pure" covalent and the "pure" ionic structures of the isothiocyanato group.[26−29] The details are discussed in a previous paper.[18] The detailed study of the other substance from this homologous series (3TCB)[18] suggests that in addition, the Davydov splitting [31] due to interaction between molecules in the unit cell can be the third reason for the complexity of the observed band.

Polymorphism of the Solid State. The IR spectra are obtained in a wide frequency range for numerous experimental runs of various thermal treatments of the sample. During the first measurement series started by cooling the sample from SmE to 30 K at the rate of 10 K/min, no changes in the IR spectra indicating crystallization are observed. Afterward, an attempt to reconstruct the sequence of phase transitions revealed by calorimetric measurement is made. The sample is heated to 250 K and then annealed at this temperature for 12 h. Due to lack of changes of IR spectra, the sample is heated to 260 K and the next annealing of sample is performed. Slight evolution of the IR spectra is registered only while the sample is annealed at 263 K and then at 275 K. The significant variation of a location of the maximum of the band corresponding to the NCS stretching mode is observed during 14 h of annealing at 285 K, and after this time, the evolution of the IR spectra ceases. The variation of the shape of the band assigned to the NSC group vibration during the sample annealing is depicted in Figure 6. In the next step, the sample is cooled from the crystalline phase at 290 to 70 K at a rate of 1 K/min. The splitting of the band in the 2400−1800 cm^{-1} range is observed, and two intensive peaks appear. They are located at 2071 and 2043 cm^{-1} at 70 K. On heating, the peaks overlap gradually. The evolution of the band shape is shown in Figure 7.

We now focus on the band corresponding to the ν_{as} (NCS) mode also analyzed in our previous studies.[18] The temperature dependence of intensities and peaks positions is plotted in Figure 8. It is evident that the intensities of both peaks decrease upon heating, and their spectral positions are shifted toward 2055 cm^{-1}. The stability of the sample at 285 K is verified by annealing for ~4.5 h. Insignificant evolution of the IR spectra is observed. Then the sample is heated to 320 K after equilibration. A two-step transition to the SmE phase is identified. The first evolution of the IR spectra is observed at 298 K. The next significant changes in the bands attributed to NCS group vibration are visible at 314 K. One can suppose that at 285 K, the mixture of two crystalline phases is obtained. The first

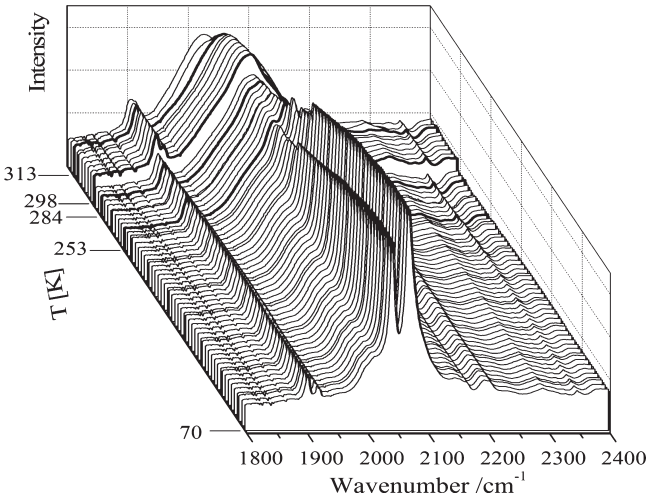

Figure 7. The temperature evolution of the IR bands corresponding to stretching vibration of the NCS group. The spectra were collected during the heating run after the sample was initially cooled to 70 K from the crystalline phase at 290 K.

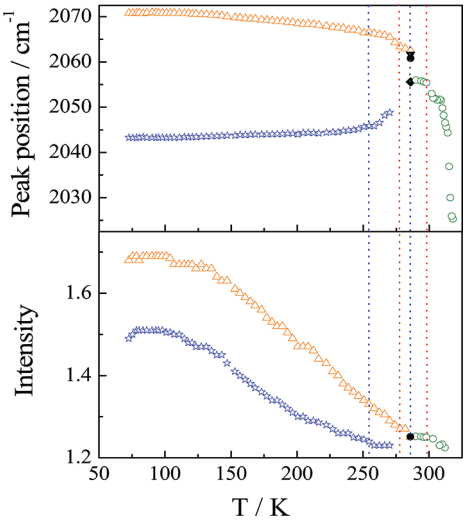

Figure 8. Temperature dependence of the location and the intensities of peaks in the 2040−1800 cm^{-1} region observed on heating. Lines mark the transition temperatures from the calorimetric measurements: dashed lines, temperatures of phase transitions of Q1 and Q2; solid lines, temperatures of phase transition of A1 and A2 obtained on heating the sample.

crystalline phase transforms to the SmE at 298 K, and the second one turns into the SmE phase at 314 K. The measurement run is repeated, with the additional annealing at 298 K . After this thermal treatment of the sample, the IR spectra evolution at 314 K is still observed.

Glass Transition and the Cold Crystallization Process. As in the case of the 3TCB sample,[5] during cooling, the SmE phase of 6TCB to 30 K, the crystallization process (phase transition(s) to low-temperature crystalline phase) is not observed in the IR spectroscopy measurement. On subsequent heating, the variation of the IR spectra analogous to those observed for 3TCB is registered. The absorption spectrum of the low-temperature phase transformed at 230 K to the spectrum of the SmE phase,

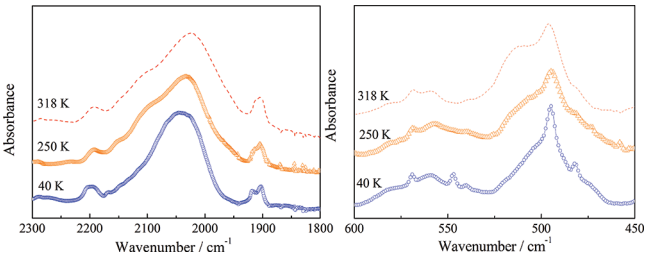

Figure 9. Profiles of the absorption spectra of the NCS vibration for a glass at 40 K, a metastable SmE phase at 250 K, and the SmE phase at 318 K.

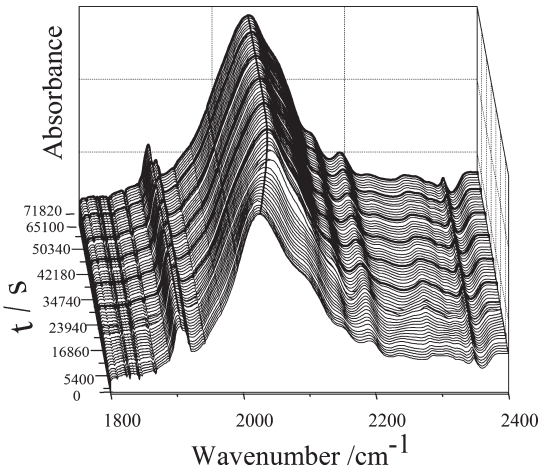

Figure 10. IR spectra in the 1800−2400 cm^{-1} region vs time during crystallization of 6TBC at 285 K.

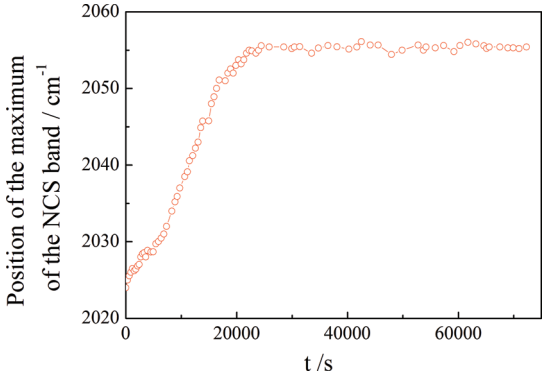

Figure 11. Location of the maximum of the NCS band in the 2400−1800 cm^{-1} region as a function of time.

and then the crystallization process at 263 K is observed. Consequently, it may be concluded that on cooling, a glassy state of the SmE phase is formed, and then on heating above the "softening" of the glass, a metastable SmE phase crystallizes (see Figure 9).

As a part of this study, the "cold" crystallization process of 6TCB was monitored. Starting with the glass at 100 K, the sample was heated to 285 K, and the IR spectra were collected continuously in real time. The time evolution of the absorption

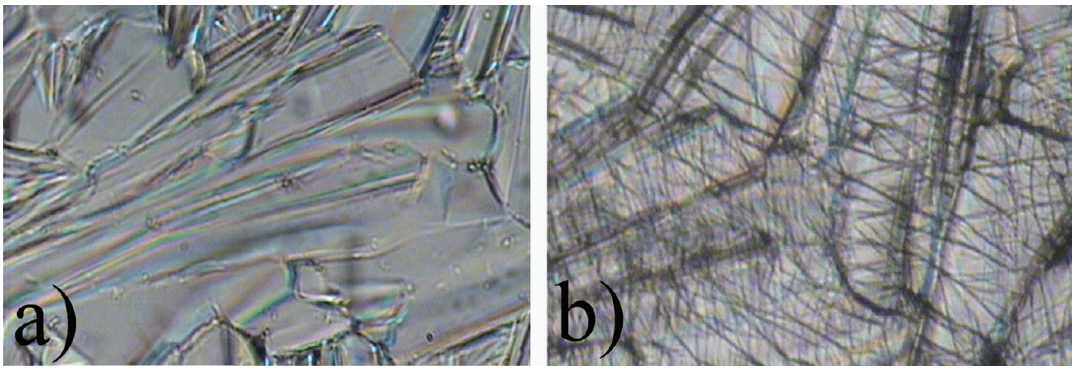

Figure 12. Textures of (a) the SmE phase at 330 K and (b) the glass of the SmE phase at 93 K. The horizontal dimension of the picture corresponds to 0.5 mm.

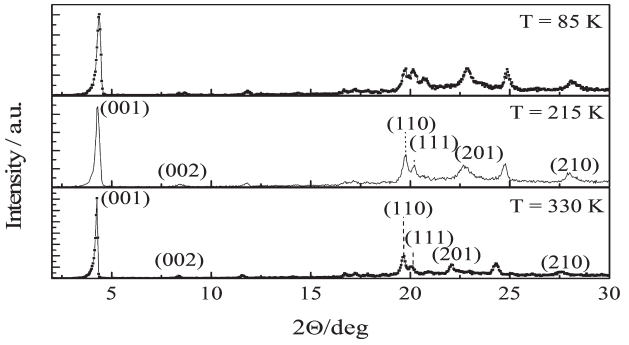

Figure 13. X-ray diffraction patterns of 6TCB collected in the SmE phase at 330 K, the metastable SmE phase at 215 K, and in the glassy phase of the SmE at 85 K.

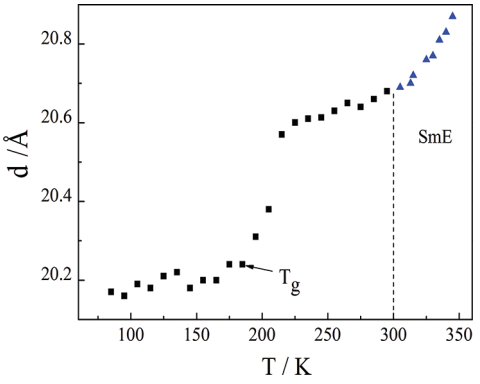

Figure 14. Temperature dependence of the smectic layer thickness for 6TCB determined from the diffraction patterns collected during heating.

spectrum corresponding to the stretching vibration of the NCS group is shown in Figure 10. It is evident in Figure 11 that on crystallization, the maximum of the NCS band in the 2400–1800 cm^{-1} region is shifted by ~30 cm^{-1} toward a higher frequency. The process lasts ~420 min. It is worth mentioning that according to dielectric measurement, after this time, the crystallinity of the sample equals ~80%. Further increase in the crystalline volume fraction is slight,[32] which is corroborated by no further shift in the IR spectra registered.

3.3. Polarized Microscopy. In addition, the glass transition is illustrated by textures obtained using polarized microscope. During cooling run for 6TCB from the SmE phase, no experimental evidence of crystallization process is observed. At a low temperature, the cracks in the texture of the SmE phase appear, then they disappear on heating above the temperature of "softening" of the glassy state (see Figure 12). Changes in the texture due to crystallization upon heating are observed around 258 K. Similar behavior is observed for the glass of the cholesteric phase of isopentylcyanobiphenyl.[32]

3.4. X-ray Studies. To record the X-ray diffraction pattern of the glassy state of SmE for 6TBC, the sample was cooled from the SmE phase (at a rate of 10 K/min) to liquid nitrogen temperature. The patterns are obtained every 10 K during heating. Figure 13 shows the examples of the X-ray pattern in the glass of the SmE phase at 85 K and in the SmE phase at 330 K. The 001 reflection is attributed to the thickness of the smectic layer-spacing, d. The temperature dependence of d depicted in Figure 14 shows a continuous variation with growth of ~0.4 Å at the softening. A similar temperature evolution of d_{001} spacing was obtained for the glass transition of 3TCB. The 110 and 111 reflections corresponding to orthorhombic molecular arrangement are broader for the low-temperature phase (presumably, the glass of SmE) in comparison with those obtained for the equilibrium SmE phase. While the sample is heated, the X-ray pattern of the low temperature phase transforms at about 200 K to the X-ray pattern characteristic for the SmE phase. One can suppose that below 200 K, the layer system of the SmE phase remains, but the orthorhombic molecular arrangement is slightly disturbed. As factors that are conducive to the formation of the vitreous state of SmE, one can consider rather loose molecular packing within the smectic layer and also partial orientational disorder of molecules in the SmE phase.

A diffraction study of the SmE phase for the *n*TCB homologous series[2,3] has pointed out that only ~60% of the unit cells are occupied by the molecular bodies that facilitated the long-range fluctuations of the molecular centers of mass. The analysis of entropy changes at the isotropic (SmE and the SmE) crystal phase transitions for *n*TCB[22] indicates partial disorder of the head-to-tail orientations of molecules and partial conformational disorder of isothiocyanato and alkyl groups in the SmE phase. The X-ray results for 6TCB are consistent with those obtained for 3TCB.[18] They support a hypothesis that the glassy state of the SmE is formed upon freezing orientational and conformational molecular disorder and positional fluctuations of the molecules within the layers.

4. CONCLUSIONS

The results of the polymorphism study of 6TCB by means of four complementary methods are reported. The calorimetry measurement reveals that the quenching of the SmE phase leads to deep supercooling of this phase. On heating the quenched SmE phase, in $C_p(T)$ an exothermic region is found. However, after special annealing of the supercooled SmE phase, the stable crystal CII is obtained transforming to crystal CI that transforms to SmE. The quantitative analysis of the IR spectra indicates that on heating of the quenched sample, softening of the glass of the SmE is observed, followed by crystallization of the metastable SmE phase. However, on heating, a two-step transition to the SmE phase is observed by IR spectroscopy not recorded by any experimental runs of the calorimetry measurement. One can suppose that the mixture of two crystalline phases is formed at 285 K and the energy necessary for active rotational freedom of molecules is different for both crystalline components. The X-ray results are consistent with those reported for 3TCB.[18] They support the hypothesis that the vitreous state of the SmE phase is formed upon freezing orientational and conformational molecular disorder and positional fluctuations of the molecules within the smectic layers. On heating, the softening of the glassy state to the SmE phase is observed, but no crystallization is detected by X-ray measurement. The glass transition was also illustrated by textures recorded using polarized microscopy. However, it is difficult to precisely identify the correspondence of sample states in different experiments because of the different sample geometries.

Despite the fact that *n*TCB compounds $(2 \leq n \leq 10)$ show the same mesophase, the alkyl chain length plays a significant role in a solid-state polymorphism. The transition temperature from the crystalline phase to the SmE phase shows the odd−even effect, that is, a pronounced alternation as the number of carbon atoms in the end chains increases. In comparison with the phase pattern in 6TCB, the lower member of this homologous series (5TCB) exhibits two stable crystalline phases, whereas in 4TCB, a deeply supercooled SmE phase and one stable crystalline phase is found. On the other hand, 3TCB shows the glassy state of the SmE phase and five crystalline phases. To elucidate how the length and conformation of the alkyl chains influence the phase pattern of the nTCB compounds, further experimental and theoretical effort is required.

APPENDIX

Table 1. The Experimental and the Calculated (B3LYP/6-311++G(d,f)) IR Spectroscopic Data for 6TCB[a]

calculated (nonscaled)		experimental frequency			
frequency	intensity	smectic E	CrII	glass of the SmE	assignment
437.297	5.5091	439	432	441	δ (NCS)
452.5789	1.3134				γ (NCS) + ν (CC)
471.1512	7.2947				ν (NCS) + ν (CC)
490.0859	5.0183		475	483	δ (NCS) + ν (NCS)
548.5825	14.5773	496	491	493	γ (NCS)
584.6156	5.9644	512			γ (CH)
646.7039	11.9688				ν (C5−C16)
666.6379	0.2021				ν^{ar} (CC) I, II
678.7748	0.1089				δ^{ar} (CC) II + ν (C2−C7)
743.8254	14.2627	726	728	729	δ^{ar} (CC) I, II + ν (C2−C7) + ν (N−C10)
753.0653	10.1608	743	741		ν^{ar} (CC) I, II + γ (CH_2) + ν (C2−C7)
754.3919	4.5928	759			ρ (CH_2)
768.8849	0.3514				ρ (CH_2)
779.1967	5.6188				γ^{ar} (CC) I, II
822.8403	0.3568				ρ (CH_2)
838.9221	26.7914				γ^{ar} (CH) I, II + ν (C5−C6)
862.6518	36.1042				γ^{ar} (CH) I, II
865.0353	36.417		761	774	γ^{ar} (CH) I, II
874.0447	0.3788				γ^{ar} (CH) II
892.0227	13.9365	781	777	778	γ^{ar} (CH) I, II
912.5647	1.5581				νar (CC) I + γ^{ar} (CH) II
916.3371	59.2779	812	810	812	ν^{ar} (CC) I + ν (NCS) + γ^{ar} (CH) II
918.5692	0.718		844	849	τ (CH_2) + γ^{ar} (CH) II
995.9567	0.3482		954	973	γ^{ar} (CH) I, II
997.4136	0.9317				γ^{ar} (CH) I, II
1001.154	0.0123				γ^{ar} (CH) I, II
1005.137	0.3195	843	855	851	γ^{ar} (CH) II
1015.708	0.6011			868	ν^{ar} (CC) + γ^{ar} (CH) II
1025.357	0.1227				τ (CH_2)
1038.467	1.3913				ν^{ar} (CC) + γ^{ar} (CH) II

Table 1. Continued

calculated (nonscaled)		experimental frequency			
frequency	intensity	smectic E	CrII	glass of the SmE	assignment
1043.703	15.264	939	933	938	ν^{ar} (CC) I, II
1055.845	1.3469	988		998	δ ^{ar} (CH) I, II
1063.45	0.0249				δ ^{ar} (CH) I, II
1068.568	0.7606	1004	1012	1009	ν (CC) + δ (CH)
1083.898	0.393				ν (CC)
1119.769	0.9411	1019	1025	1022	τ (CH_2) + δ^{ar} (CH) II
1152.627	17.4001	1045	1047		ν (CC) + ω (CH_3)
1160.611	5.9366	1054	1056	1059	ν (CC) + δ (CH)
1234.425	0.3784	1108	1108	1112	δ^{ar} CH) I
1244.767	7.253	1139	1137	1141	δ^{ar} (CH) II
1252.414	0.3885	1148		1147	ω (CH_2)
1256.167	1.3165				ν^{ar} (CC) I, II
1292.512	0.2024	1181	1181	1180	ν^{ar} (CC) I, II
1296.861	0.6124			1191	ν (NCS) + ν (CC)
1300.204	0.3438	1190		1995	ν^{ar} (CC) I, II
1329.914	2.5785	1205	1214		ν^{ar} (CC) I, II
1332.927	1.3235				ν^{ar} (CC) I, II
1337.247	0.3417	1221	1225	1229	τ (CH_2)
1349.552	0.4896				τ (CH_2)
1352.311	0.6501		1256	1266	ρ (CH_2)
1355.635	0.4823	1280	1274	1277	ν^{ar} (CC) I, II
1357.7	1.1303		1285	1286	τ (CH_2)
1375.887	0.7987				δ^{ar} (CH) I
1390.192	0.1901		1299	1299	δ^{ar} (CH) II
1409.169	0.5455	1307	1315	1315	ω (CH_2)
1414.59	1.5824	1323	1321	1324	ω (CH_2)
1455.785	6.8807	1380	1378	1383	ν^{ar} (CC) I, II
1459.83	2.7676	1401	1398	1404	δ (CH_3) s
1479.403	0.9773				δ ^{ar} (CH) I, II
1531.658	0.176				δ^{sci} (CH_2)
1532.964	0.1818	1422	1420	1422	δ^{sci} (CH_2)
1537.081	0.9288				δ^{sci} (CH_2)
1543.423	2.4814				δ^{sci} (CH_2)
1544.67	7.7596	1439	1432	1435	δ (CH_3) s
1552.522	1.0575				δ (CH_2) + δ (CH_3) s
1554.555	121.9085	1452	1460	1464	ν (CC)
1560.559	7.5872	1460	1460	1464	δ_{sci} (CH_2)
1578.475	1.478	1495	1497	1502	ν^{ar} (CC) I, II
1599.869	0.1601				ν^{ar} (CC) I, II
1624.322	0.4664	1547	1549	1552	ν^{ar} (CC) I, II
1661.033	0.2322	1569	1568	1571	ν^{ar} (CC)I
1671.642	6.4086	1598	1597	1602	ν^{ar} (CC)I, II
2251.704	1900.895	2025	2035	2069	ν (NCS)
				2041	
		1906	1911	1920	
3007.253	1.2698				ν (CH_2)s
3010.882	8.4101				ν (CH_2)s
3021.863	27.95	2844	2836	2840	ν (CH_2)s
3024.95	30.5294	2855	2852	2852	ν (CH_2)s
3031.031	0.2875				ν (CH_2)s
3035.185	90.9004				ν (CH_2)s
3036.272	59.5445				ν (CH_3)s

Table 1. Continued

calculated (nonscaled)		experimental frequency			
frequency	intensity	smectic E	CrII	glass of the SmE	assignment
3042.679	0.4242				ν (CH_2)as
3057.688	2.7105				ν (CH_2)as
3070.291	24.4736				ν (CH_2)as
3088.467	81.7056	2925	2924	2919	ν (CH_2)as
3109.251	77.8683	2958	2955	2952	ν (CH_2)as
3113.999	51.4101				ν (CH_3)as
3185.89	8.7429				ν^{ar} (CH) II as
3186.706	39.1215	3032	3026	3030	ν^{ar} (CH) II as
3207.605	20.341	3055	3053	3061	ν^{ar} (CH) I, II as
3210.628	8.484				ν^{ar} (CH) I, II as
3214.282	9.8906				ν^{ar} (CH) I, II as
3215.304	9.872				ν^{ar} (CH) I, II s
3232.392	13.2195	3096	3097	3101	ν^{ar} (CH) I s
3235.219	0.7945	3112			ν^{ar} (CH) I s

[a] The particular symbols denote the following vibrations: ν, stretching; δ, in-plane deformation; δ^{sci}, scissoring; ρ, rocking; γ, out-of plane deformation; τ, twisting; ω, wagging, and the additional details: ar, ring; s, symemetric; as, asymmetric; I and II, phenyl rings (see Figure 5).

Table 2. The Main Structure Parameters of the 6TCB Molecule Optimized by DFT/B3LYP/631 Method

Bond Lengths/Å	
S−C(14)	1.642
C(14)−N	1.189
N−C(1)	1.378
C(10)−C(11)	1.407
C(11)−C(12)	1.392
C(2)−C(7)	1.482
C(5)−C(16)	1.515
C(18)−C(19)	1.539
C(19)−C(20)	1.54
C(20)−C(21)	1.537
Bond Angle/deg	
N−C(17)−S	180.0
N−C(1)−C(6)	120.157
C(2)−C(7)−C(8)	121.101
C(3)−C(2)−C(7)	121.094
C(6)−C(5)−C(16)	121.077
C(4)−C(5)−C(15)	121.075
C(5)−C(16)−C(17)	113.098
Torsion Angle/deg	
C(1)−C(2)−C(7)−C(8)	35.562
C(6)−C(5)−C(16)−C(17)	89.327
C(11)−C(10)−N−C(14)	19.611

AUTHOR INFORMATION

Corresponding Author

*E-mail: malgorzata.jasiurkowska@ifj.edu.pl.

REFERENCES

(1) Urban, S.; Czupryński, K.; Dąbrowski, R.; Janik, J.; Kresse, H.; Schmalfuss, H. *Liq. Cryst.* **2001**, *28*, 691–696.

(2) Jasiurkowska, M.; Budziak, A.; Czub, J.; Massalska-Arodź, M.; Urban, S. *Liq. Cryst.* **2008**, *35*, 513–518.

(3) Jasiurkowska, M.; Budziak, A.; Czub, J.; Urban, S. *Acta Phys. Polon. A* **2006**, *110*, 795–805.

(4) Urban, S.; Przedmojski, J.; Czub, J. *Liq. Cryst.* **2005**, *32*, 619–624.

(5) Dąbrowski, R.; Przedmojski, J.; Spadło, A.; Dziaduszek, J.; Tykarska, M. *Phase Trans.* **2004**, *77*, 1103–1110.

(6) Massalska-Arodź, M.; Würfinger, A.; Büsing, D. *Naturforsch.* **1999**, *54a*, 675–678.

(7) Massalska-Arodź, M.; Schmalfuss, H.; Witko, W.; Kresse, H.; Würfinger, A. *Mol. Cryst. Liq. Cryst.* **2001**, *366*, 221–227.

(8) Urban, S.; Würflinger, A.; Kocot, A. *Liq. Cryst.* **2001**, *28*, 1331–1336.

(9) Urban, S.; Würflinger, A. *Z. Naturforsch.* **2002**, *57a*, 233–236.

(10) Urban, S.; Würflinger, A. *Phys. Rev. E* **2005**, *72*, 021707–021707−4.

(11) Ishimaru, I.; Saito, K.; Ikeuchi, S.; Massalska-Arodź, M.; Witko, W. *J. Phys. Chem. B* **2005**, *109*, 10020–10024.

(12) Urban, S.; Czub, J.; Dąbrowski, R.; Kresse, H. *Liq. Cryst.* **2005**, *32*, 119–124.

(13) Drozd-Rzoska, A.; Rzoska, S. J.; Czupryński, K. *Phys. Rev. E* **2000**, *61*, 5355–5360.

(14) Drozd-Rzoska, A.; Rzoska, S. J.; Zioło, J.; Jadżyn, J. *Phys. Rev. E* **2000**, *61*, 052701–052701-4.

(15) Mukherjee, P. K. *Phys. Lett. A* **2007**, *365*, 483–488.

(16) Mukherjee, P. K.; Rzoska, S. J. *Phys. B* **2007**, *400*, 292–296.

(17) Pełka, R.; Yamamura, Y.; Jasiurkowska, M.; Massalska-Arodź, M.; Saito, K. *Liq. Cryst.* **2008**, *35*, 179–186.

(18) Jasiurkowska, M.; Ściesiński, J.; Massalska-Arodź, M.; Czub, J.; Pełka, R.; Juszyńska, E; Yamamura, Y.; Saito, K. *J. Phys. Chem. B* **2009**, *113*, 7435–7442.

(19) Gray, G. W.; Goodby, J. W. G. *Smectic Liquid Crystal Texture and Structure*; Leonard Hill: Glasgow, 1984.

(20) Dierking, I. *Textures of Liquid Crystals*, Wiley-VCH Verlag: Weinheim, 2003.

(21) Edited by Demus, D., Goodby, J., Gray, G. W., Spiess, H.-W., Vill, V. *Handbook of Liquid Crystals*; Wiley-VCH Verlag: Weinheim, 1998.

(22) Horiuchi, K.; Yamamura, Y.; Pełka, Y.; Sumita, M.; Yasuzuka, S.; Massalska-Arodz, M.; Saito, K. *J. Phys. Chem. B* **2010**, *114*, 4870–4875.

(23) Yamamura, Y.; Saito, K.; Saitoh, H.; Matsuyama, H.; Kikuchi, K.; Ikemoto, I. *J. Phys. Chem. Solids* **1995**, *56*, 107–115.

(24) Rogers, D. W. *Computational Chemistry Using the PC*; John Wiley & Sons: Hoboken, NJ, 2003.

(25) Vreven, T.; Frisch, M. J.; Kudin, K. N.; Schlegel, H. B.; Morokuma, K. *Mol. Phys.* **2006**, *104*, 701.
(26) Kupka, T.; Warzlik, R.; Pasterna, G.; Pasterny, K. *J. Mol. Struct.* **2002**, *616*, 17–32.
(27) Campbell, N. L.; Gillis, C. J.; Klapstein, D.; Nau, W. M. *Spectrochim. Acta* **1995**, *51A*, 787–798.
(28) During, J. R.; Chao, Z.; Deeb, H. *J. Mol. Struct.* **2006**, *784*, 78–92.
(29) Majewska, P.; Rospenk, M.; Czarnik-Matusewicz, B.; Sobczyk, L. *Chem. Phys.* **2007**, *334*, 117–127.
(30) Majewska, P.; Rospenk, M.; Czarnik-Matusewicz, B.; Kochel, A.; Sobczyk, L.; Dąbrowski, R. *Chem. Phys.* **2007**, *340*, 227–236.
(31) Davydov, A. S., *Theory of Molecular Excitions*; McGraw-Hill Book Company: New York, 1962.
(32) Mayer, J.; Witko, W.; Massalska-Arodź, M.; Williams, J.; Dąbrowski, R. *Phase Trans.* **1999**, *68*, 199–213.